GEOPHYSICS, VOL. 75, NO. 6 (NOVEMBER-DECEMBER 2010); P. N97–N107, 9 FIGS.
10.1190/1.3484155

Low-frequency fluid waves in fractures and pipes

Valeri Korneev[1]

ABSTRACT

Low-frequency analytical solutions have been obtained for phase velocities of symmetrical fluid waves within both an infinite fracture and a pipe filled with a viscous fluid. Three different fluid wave regimes can exist in such objects, depending on the various combinations of parameters, such as fluid density, fluid viscosity, walls shear modulus, channel thickness, and frequency. Equations for velocities of all these regimes have explicit forms and are verified by comparisons with the exact solutions. The dominant role of fractures in rock permeability at field scales and the strong amplitude and frequency effects of Stoneley guided waves suggest the importance of including these wave effects into poroelastic theories.

INTRODUCTION

We consider and compare the propagation of a fundamental symmetrical mode (fluid wave) for two model geometries: a fracture and a pipe, both infinite along the symmetry axis, filled with viscous fluid, and surrounded by an unbounded elastic medium. The importance of this fluid wave is well-established for boreholes (tube wave) and supported by numerical modeling results for fractures (Groenenboom and Fokkema, 1998; Ziatdinov et al., 2006; Korneev et al., 2009; Frehner and Schmalholz, 2010; Derov et al., 2009), indicating the dominant role of this wave in wave propagation phenomena in saturated rock. In Korneev (2008), it was found that in fractures filled with viscous fluid, a fluid wave can propagate in different regimes. While in one regime the dispersion exists only in viscous fluids and does not depend on wall elastic parameters, for the other regime the fluid wave is dispersive, even for zero fluid viscosity, and depends on the wall's shear modulus. The third regime takes place at the zero limit of a fracture thickness. Relationships between these regimes remain unclear: What are the conditions of their existence? What is the difference between fractures and pipes in fluid wave propagation? In this paper, we derive the simple analytical conditions for these three different propagation regimes within both of the considered geometries and present explicit analytical expressions for the correspondent phase velocities. Hereafter, we refer to a *channel* when addressing fluid-containing parts for both a fracture and a pipe, which is a useful notation for discussion of similarities and differences between them.

THEORY FOR A FRACTURE

Previous work

The Stoneley guided wave, which propagates in a fluid layer bounded by elastic walls, was first obtained as a mathematical result by Krauklis (1962). Paillet and White (1982) re-derived that solution while comparing waves in a borehole and its 2D analogue. Their solution has an implicit form as a fundamental symmetric mode that propagates along the fracture, with a velocity approaching zero at zero frequency.

Fluid-filled fracture waves have also been investigated, both numerically and in laboratory studies to explain volcanic tremors and for monitoring hydraulic fracturing (Chouet, 1986, 1988; Ferazzini and Aki, 1987; Ferrazzini et al., 1990; Tang and Cheng, 1988; Goloshubin et al., 1994; Groenenboom and Falk, 2000; Groenenboom and van Dam, 2000; Yamamoto and Kawakatsu, 2008). Fluid waves are essential in generating tube-wave reflections from intersecting fractures (Hornby et al., 1989; Kostek et al., 1998a, b; Derov et al., 2009; Ziatdinov et al., 2006). The high amplitudes of such waves make the solution of relevant problems rather simple because we can ignore most other types of waves without compromising the result. Because of the low velocity of fluid waves at low frequencies, the fluid-filled channels are capable of trapping wave energy and carrying it for long distances, exhibiting waveguide features. Propagation of the Stoneley guided waves in a fracture filled with viscous fluid was described in Korneev (2008). In the latest developments on the subject, Frehner and Schmalholz (2010) modeled these waves for intersecting fractures using a finite-element method, and Korneev et al. (2009) compared analytical results with those obtained using OASES software.

Manuscript received by the Editor 7 August 2009; revised manuscript received 31 March 2010; published online 2 December 2010.
[1]Lawrence Berkeley National Laboratory, Berkeley, California, U.S.A. E-mail: vakorneev@lbl.gov.
© 2010 Society of Exploration Geophysicists. All rights reserved.

Fluid waves in a fracture

Here, we consider all low-frequency symmetrical fluid waves using the results from Korneev (2008) but change some notations to make them uniform with a similar problem for a cylindrical pipe. The symmetric model consists of a layer, $-h/2 \le z \le h/2$, filled with viscous fluid between two homogeneous elastic half-spaces comprised of the same material. The index $j = 1$ indicates the parameters and fields related to the viscous fluid layer, while index $j = 2$ indicates the values related to elastic half-spaces.

In both media, the relationship between the body wave velocities and media parameters is the same: a longitudinal (P-) wave propagating with velocity

$$V_{\mathrm{P}j} = \sqrt{\frac{\lambda_j + 2\mu_j}{\rho_j}} \tag{1}$$

and a shear (S-) wave with velocity

$$V_{\mathrm{S}j} = \sqrt{\frac{\mu_j}{\rho_j}}, \tag{2}$$

expressed through Lame constants λ_j, μ_j, and density ρ_j ($j = 1,2$). We assume that $V_{\mathrm{P}2} > V_{\mathrm{S}2} > V_{\mathrm{P}1}$, which is the most common case for rocks at depth.

The linearized equation of motion for compressible viscous fluid takes the form (Korneev, 2008)

$$\frac{\partial^2 \mathbf{u}}{\partial t^2} - \frac{\eta}{\rho_f}\nabla^2\frac{\partial \mathbf{u}}{\partial t} - \frac{1}{\rho_f}\left(\zeta - \frac{\eta}{3}\right)\nabla\nabla\cdot\frac{\partial \mathbf{u}}{\partial t} - c_P^2\nabla\nabla\cdot\mathbf{u} = 0, \tag{3}$$

with the particle velocity $\mathbf{u}$, time t, fluid density $\rho_f = \rho_1$, viscosity coefficients η, ζ, and speed of sound c_P for the zero-viscosity limit.

Using the time dependence of the fields in the form $\exp(-i\omega t)$, with angular frequency ω, equation 3 describes the propagation of dissipating P- and S-waves with complex velocities

$$V_{\mathrm{P}1} = \sqrt{c_P^2 - i\frac{\omega}{\rho_f}\left(\zeta + \frac{4\eta}{3}\right)}, \tag{4}$$

$$V_{S1} = \sqrt{-\frac{i\omega\eta}{\rho_f}}, \tag{5}$$

and complex Lame constants

$$\lambda_1 = c_P^2\rho_f - i\omega\left(\zeta - \frac{2\eta}{3}\right), \tag{6}$$

$$\mu_1 = -i\omega\eta. \tag{7}$$

We seek a solution in the form of a surface wave with wavenumber $k_x = \frac{\omega}{\mathrm{v}_f}$, propagating along the x axis with phase velocity v_f.

Velocities in both media have corresponding wavenumbers

$$k_{Pj} = \omega/V_{Pj}, \quad k_{Sj} = \omega/V_{Sj}. \quad (j = 1,2). \tag{8}$$

Continuity conditions for the two components of both stress and displacement at the boundaries $z = \pm h/2$ lead to four linear equations for coefficients of those components. The dispersion equation for symmetric modes is obtained by finding values of v_f for which the determinant of the system is zero

$$\begin{aligned}\alpha_{s1}[&-(1-c)^2\xi_1\xi_2\alpha_{p2}\alpha_{s2}k_x^2 - (b-c)^2\xi_1\chi_1 - ic(k_x - a)\\ &\times(k_x - b)k_x(\alpha_{p2}\chi_1 + \xi_1\alpha_{s2}) + k_x^2(k_x - ac)^2\alpha_{p2}\alpha_{s2}\\ &+ k_x^2(ca - b)^2] = 0,\end{aligned} \tag{9}$$

where

$$\xi_1 = \mathrm{i}\alpha_{P1}\tanh\left(i\alpha_{P1}\frac{h}{2}\right), \tag{10}$$

$$\chi_1 = \mathrm{i}\alpha_{S1}\coth\left(i\alpha_{S1}\frac{h}{2}\right), \tag{11}$$

$$\alpha_{Pj} = \sqrt{k_{Pj}^2 - k_x^2}, \quad \alpha_{sj} = \sqrt{k_{sj}^2 - k_x^2}, \quad (j = 1,2) \tag{12}$$

and coefficients a, b, and c have expressions

$$a = k_x\left(1 - \frac{\mathrm{v}_f^2}{2V_{S1}^2}\right), \quad b = k_x\left(1 - \frac{\mathrm{v}_f^2}{2V_{S2}^2}\right), \quad c = \frac{\mu_1}{\mu_2}. \tag{13}$$

In equation 9, the factor in square brackets is exactly that of equation 22 from Korneev (2008). The factor α_{S1} in equation 9 gives an extra root for the fluid wave propagating with the (rather small) velocity of the shear wave in viscous fluid, given by equation 5. Low-frequency approximation means that both frequency ω and thickness h are small enough to provide the conditions

$$\left|\alpha_{P1}\frac{h}{2}\right| \ll 1, \quad \left|\alpha_{P2}\frac{h}{2}\right| \ll 1 \quad \text{and} \quad \left|\alpha_{S2}\frac{h}{2}\right| \ll 1, \tag{14}$$

which reduces the equation for the roots of the square brackets factor in equation 9 to

$$\chi_1\left[\mathrm{k}_x h\left(1 - \frac{\mathrm{v}_f^2}{V_{P1}^2}\right) - \frac{\rho_f \mathrm{v}_f^2}{\rho_2(1-\gamma^2)V_{S2}^2}\right] = 2. \tag{15}$$

Approximating χ_1 in equation 15 by the truncated Taylor series of the *coth* function

$$\chi_1 \approx \frac{2}{\mathrm{k}_x h}\left(1 - \frac{\mathrm{k}_x^2 h^2}{12}\frac{\mathrm{v}_f^2}{V_{S1}^2}\right), \tag{16}$$

we get the cubical polynomial equation

$$\mathrm{v}_f^3 + \frac{V_{S0}^3}{V_P^2}\mathrm{v}_f^2 - \frac{V_{S0}^3 V_{B0}^2}{V_P^2 + V_{B0}^2} = 0, \tag{17}$$

for determining v_f.

Equation 17 contains three parameters, all of which are velocities with the forms (Korneev, 2008)

$$1. \quad V_{S0} = \left(\frac{\omega h \mu_2}{\rho_f}(1-\gamma^2)\right)^{\frac{1}{3}}, \tag{18}$$

(a low-frequency Stoneley guided wave velocity in a fracture filled with nonviscous fluid, where $\gamma = V_{S2}/V_{P2}$);

$$2. \quad V_{\mathrm{BF}} = V_{P1}\sqrt{\frac{-i\omega\kappa_{fr}\rho_f}{\eta}}, \tag{19}$$

(a low-frequency fluid wave velocity in a fracture with rigid walls, where $\kappa_{fr} = h^2/12$ is fracture permeability); and

$$3. \quad V_{\mathrm{P}} \equiv V_{P1}, \tag{20}$$

(a P-wave velocity in the fluid from equation 4).

Equation 17 has three roots, which can be explicitly found using the Cardano formula (Abramowitz and Stegun, 1972). Among these three roots, only one has a positive real part and therefore describes a physical wave. However, the structure of equation 17 allows for finding its asymptotic solutions in a straightforward way. If the second term in equation 17 is much smaller than the first term, then

$$\mathrm{v}_f = V_{\mathrm{S}} \equiv V_{S0} \sqrt[3]{\frac{V_{BF}^2}{V_P^2 + V_{BF}^2}}. \tag{21}$$

Substitution of equation 21 into equation 17 shows that the second term is much smaller than the first one when

$$|V_{\mathrm{S}}| \gg \left| \frac{V_{S0}^3}{V_P^2} \right|. \tag{22}$$

If in equation 21,

$$|V_P^2| \ll |V_{BF}^2|, \quad \text{or } 1 \ll \frac{\omega \kappa_{fr} \rho_f}{\eta} = \left(\frac{h}{S}\right)^2, \tag{23}$$

where viscous skin depth

$$S = \sqrt{\frac{12\eta}{\omega \rho_f}} \tag{24}$$

is much smaller than fracture thickness, the elastic forces dominate viscous ones, and the fluid wave

$$\mathrm{v}_f \approx V_{\mathrm{SF}} \equiv V_{S0}\left(1 - \frac{i\omega \kappa_{fr} \rho_f}{3\eta}\right), \tag{25}$$

propagates as the Stoneley guided wave with some attenuation. This regime exists for "thick" fractures and/or low fluid viscosity.

If, in equation 21,

$$|V_P^2| \gg |V_{BF}^2|, \quad \text{or } 1 \gg \left(\frac{h}{S}\right)^2, \tag{26}$$

then viscous forces are becoming dominant and

$$\mathrm{v}_f = V_{NF} \equiv \sqrt[3]{\frac{V_{B0}^2}{V_P^2}} = h \sqrt[3]{-i\frac{\omega^2 \mu_2}{12\eta}(1-\gamma^2)}, \tag{27}$$

which was called a "thin" fracture regime in Korneev (2008).

If, in equation 17, the second term dominates over the first term, then

$$\mathrm{v}_f = V_B \equiv \frac{V_{\mathrm{P}} V_{\mathrm{BF}}}{\sqrt{V_P^2 + V_{BF}^2}}. \tag{28}$$

Substitution of equation 28 into equation 17 reveals that the second term is much larger than the first one when

$$|V_B| \gg \left| \frac{V_{S0}^3}{V_P^2} \right|. \tag{29}$$

At low frequencies (inequalities 26), equation 28 gives

$$\mathrm{v}_f = V_{\mathrm{BF}} = V_{P1} \sqrt{\frac{-i\omega \kappa_{fr} \rho_f}{\eta}}, \tag{30}$$

which is a propagation in a regime when interaction of the fluid wave with the fracture walls occurs exclusively through viscous friction forces.

At high frequencies, when the inequalities 23 take place, equation 28 gives

$$\mathrm{v}_f \approx V_{\mathrm{P}}, \tag{31}$$

which is the propagation of body P-waves in the fluid.

Velocities V_{SF}, V_{BF}, and V_{NF} correspond to three different regimes of fluid wave propagation in a fracture, where subscript F indicates their relation to the fracture model. Similar regimes also can exist for a fluid wave in a pipe.

After simple algebra, it is easy to demonstrate that inequality 22 associated with the solution 21 is equivalent to

$$|V_{\mathrm{S}}| \ll |V_B|, \tag{32}$$

and that the inequality 29 associated with solution 28 is equivalent to

$$|V_{\mathrm{S}}| \gg |V_B|, \tag{33}$$

which is exactly opposite to the inequality 32.

The inequalities 32 and 33 mean that for any parameter set, a wave propagation regime corresponds to a regime with the slowest velocity. The regime change occurs when

$$|V_{\mathrm{S}}| \approx |V_B|. \tag{34}$$

Thus, when

$$|V_{\mathrm{S}}| > |V_{\mathrm{P}}|, \tag{35}$$

the wave propagates with the velocity of P-waves in the fluid (equation 31). If both V_{S} and V_B are less than $|V_{\mathrm{P}}|$ then, after substitution of expressions 21 and 28 into equation 34, we obtain

$$\omega_T \approx \frac{1}{h}\left[\sqrt{\left(\frac{6\eta}{h\rho_f}\right)^2 + \left(\frac{\rho_f |V_P^3|}{\mu_2(1-\gamma^2)}\right)^2} - \frac{6\eta}{h\rho_f}\right] \tag{36}$$

for a transitional frequency ω_T that separates different propagation regimes.

For thick fractures and small viscosities, when

$$\left(\frac{h\rho_f^2 |V_P^3|}{6\eta\mu_2(1-\gamma^2)}\right)^2 \gg 1, \tag{37}$$

a transition between V_{SF} and V_{BF} regimes takes place, and equation 36 becomes

$$\omega_T \approx \frac{\rho_f |V_P^3|}{h\mu_2(1-\gamma^2)}. \tag{38}$$

If the inequality sign in equation 37 is reversed (a case of a thin fracture or large viscosity), then

$$\omega_T \approx \frac{|\lambda_1^3|}{12\eta\mu_2^2(1-\gamma^2)^2}, \tag{39}$$

and the transition occurs between V_{BF} and V_{NF} regimes.

NUMERICAL RESULTS FOR A FRACTURE

The derived exact and asymptotic solutions were compared numerically for a set of media models with different parameters. The exact solution was obtained by a direct root search when the left-hand side of equation 9 was computed on a dense grid for complex velocity v_f. Both the real and imaginary parts varied from zero to a value exceeding velocity in the fluid. The computed function was analyzed numerically, always revealing the presence of two roots. One root corresponded to the velocity of shear waves in the fluid; the other root numerically coincided with the only physical solution of equation 17, which was computed using Cardano formulas. Among the three roots of equation 17, just one has a positive real part, giving the only physically interpretable estimate for the exact solution of equation 9. The asymptotic solutions 25, 27, and 28 were compared with the exact solutions. For all examples presented here, the parameters of the elastic medium were $V_{P2} = 5000$ m/s, $V_{S2} = 3000$ m/s, and $\rho_2 = 2.7$ g/cm^3. Figure 1 shows the real part of the phase velocities as the functions of density. The parameters of the model are $c_P = 1500$ m/s, the viscosities $\eta = \varsigma = 1$ cP, frequency 20 Hz, $c_P = 1500$ m/s, and the fracture thickness 10^{-3} m. At low densities, the exact solution follows the solution for the V_{BF} regime, while at higher densities, it follows the V_{SF} regime. Note that the transition between these two regimes corresponds to the condition from equation 34.

In Figures 2–6, the function V_{BF} is shown instead of function V_{BF} to demonstrate a transition of this regime into propagation of P-body wave (equation 31). Figure 2 shows phase velocities as a function of frequency when the fluid has the same parameters as the "air" at at-

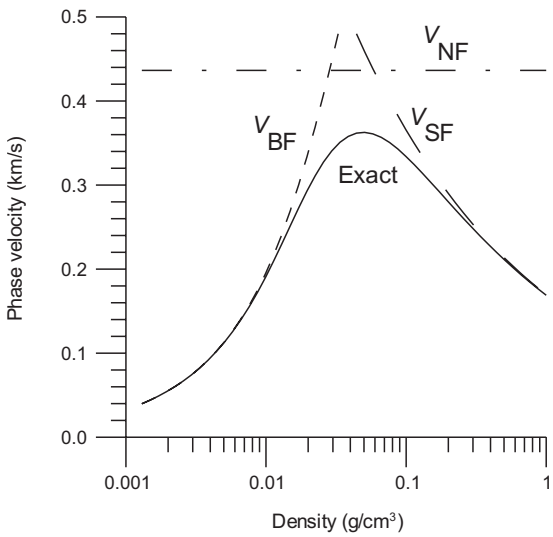

Figure 1. Real part of phase velocity of fluid wave in a 10^{-3} m thick fracture as a function of fluid density. The fluid has sound velocity of 1500 m/s and viscosity of 1 cP; the frequency is 20 Hz. Shown are the exact solution (solid line) obtained from equation 9, V_B (short dashed line, equation 28), V_{SF} (long dashed line, equation 25), and V_{NF} (dashed-dotted line, equation 27).

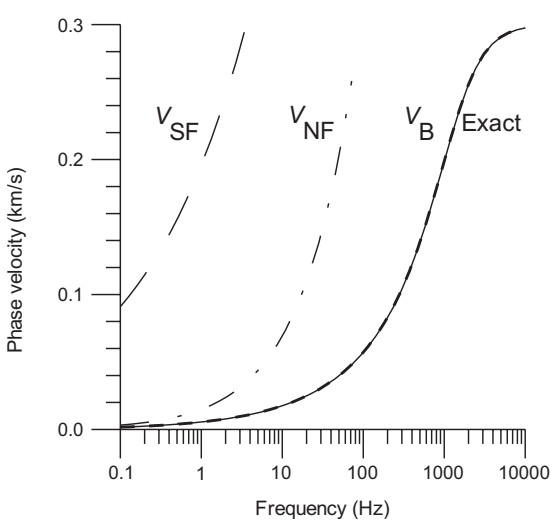

Figure 2. Real part of phase velocity of fluid wave in a 10^{-3} m thick fracture as a function of frequency for the "air" at atmospheric pressure. The curves marked as on Figure 1. Solution V_B gives accurate approximation to the exact solution.

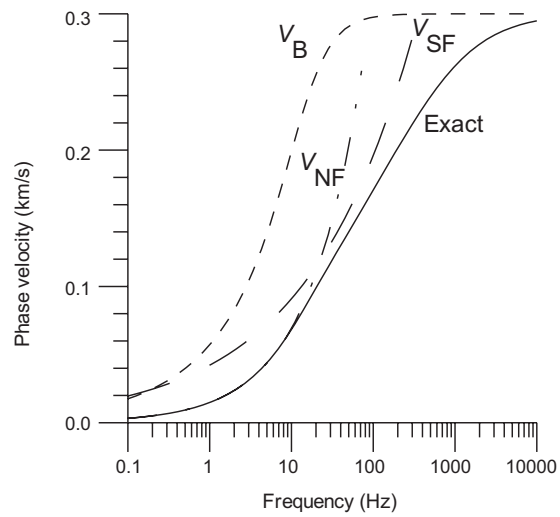

Figure 3. Real part of phase velocity of fluid wave in a 10^{-4} m thick fracture as a function of frequency for the air at 10 MPa pressure. The curves marked as on Figure 1. At low frequencies, the V_{NF} regime approximates the exact solution.

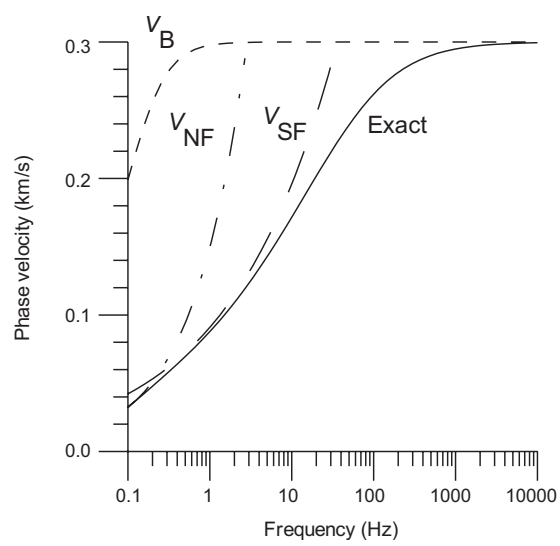

Figure 4. Real part of phase velocity of fluid wave in a 10^{-3} m thick fracture as a function of frequency for the air at 10 MPa pressure. The curves marked as on Figure 1. For most frequencies, the exact solution is in transitional regimes.

mospheric pressure, when $c_P = 330$ m/s, $\rho_f = 0.0013$ g/cm^3, and $\eta = \varsigma = 1$ cP. Here, the exact solution accurately follows the V_{BF} regime solution; however, for a fracture 10 times thinner ($h = 10^{-4}$ m), the V_{NF} regime takes place at low frequencies (Figure 3). The case for air compressed at 10 MPa (hydrostatic pressure at ~1 km depth) is shown in Figure 4, where $\rho_f = 0.13$ g/cm^3 and $h = 10^{-3}$ m. In this set of parameters, the dispersion curve belongs to a transition between the V_{SF} regime and the high-frequency solution (equation 31). The water-filled fracture case with $c_P = 1500$ m/s, $\rho_f = 1.0$ g/cm^3, $\eta = \varsigma = 1$ cP, and $h = 10^{-3}$ m is shown in Figure 5. Results for an oil-filled fracture when all the parameters have the same values as in Figure 5, except that viscosities $\eta = \varsigma = 10$ cP, are shown in Figure 6. For the seismic range of frequencies, the solutions for water and oil are well represented by V_{SF} regime.

We will discuss these results together with similar results for a pipe — the subject of the next section.

THEORY FOR A PIPE

Previous work

Fluid-filled boreholes are one of the most important signal-carrying channels in prospecting geophysics, and the literature on the properties of borehole fluid waves is quite extensive (Burridge et al., 1993, Schoenberg et al., 1981, Cheng and Toksoz, 1981; Chang et al., 1988; Haddon, 1989; Norris, 1989, etc.). Tube waves (Stoneley waves in a pipe) are used for permeability logging, fracture detection, reservoir monitoring, and borehole integrity testing. The similarity of Stoneley waves to Biot slow waves has been noted (Chang et al., 1988); Norris (1987) even described the tube wave as "a limiting case of the Biot slow wave." In poroelastic theory (Biot, 1956b), it is assumed that on a pore scale, the channel walls are rigid and a fluid wave in a cylindrical pipe is a core model for fluid-solid interaction. In reality, however, values of liquid rigidity are comparable with those of elastic rock, and therefore wall-rigidity assumptions need to be evaluated, as was done for the case of fractures in the previous section. Here, we revisit the problem of low-frequency wave propagation in a cylindrical pipe filled with viscous fluid and demonstrate the existence of three fluid wave propagation regimes similar to those found in the fracture model.

Fluid waves in a pipe

We are interested in the low-frequency properties of purely symmetric fluid waves propagating along a thin cylindrical well (or a pipe) filled with viscous fluid. Outside of a cylinder with radius R, the medium is elastic. In the following, index $j = 1$ refers to a fluid, while index $j = 2$ denotes an elastic medium. Here, we also use notations introduced in equations 1–8.

It is assumed that longitudinal (P-) and shear (S-) waves in both media of the pipe satisfy welded boundary conditions at the pipe wall, providing continuity for stresses and displacements. (Mathematical formalism and the main expressions for wave propagation problems with cylindrical symmetry are presented in Appendix A). The pure symmetry of the problem leaves only terms with m = 0 in the general field expansion (equation A-6). As a result, the propagation velocities v_f of the fluid waves can be found as the roots of the equation

$$\alpha_{s1}\begin{vmatrix} -\xi_1 & -k_z\chi_1 & \xi_2 & k_z\chi_2 \\ -k_z & \alpha_{s1} & k_z & -\alpha_{s2} \\ q_{31} & q_{32} & q_{33} & q_{34} \\ q_{34} & q_{42} & q_{43} & q_{44} \end{vmatrix} = 0$$

$$\begin{aligned} q_{31} &= 2\mu_1 k_z \xi_1, & q_{32} &= \mu_1(2\alpha_{s1}^2 - k_z^2)\chi_1 \\ q_{33} &= 2\mu_2 k_z \xi_2, & q_{34} &= -\mu_2(2\alpha_{s2}^2 - k_z^2)\chi_2 \\ q_{41} &= \lambda_1 k_{p1}^2 + 2\mu_1\alpha_{p1}^2\left(1 - \frac{\xi_1}{\alpha_{p1}R}\right), & q_{42} &= 2\mu_1 k_z\left(1 - \frac{\chi_1}{\alpha_{s1}R}\right), \\ q_{43} &= -\lambda_2 k_{p2}^2 - 2\mu_2\alpha_{p2}^2\left(1 - \frac{\xi_2}{\alpha_{p2}R}\right), & q_{44} &= -2\mu_2 k_z\left(1 - \frac{\chi_2}{\alpha_{s2}R}\right). \end{aligned} \tag{40}$$

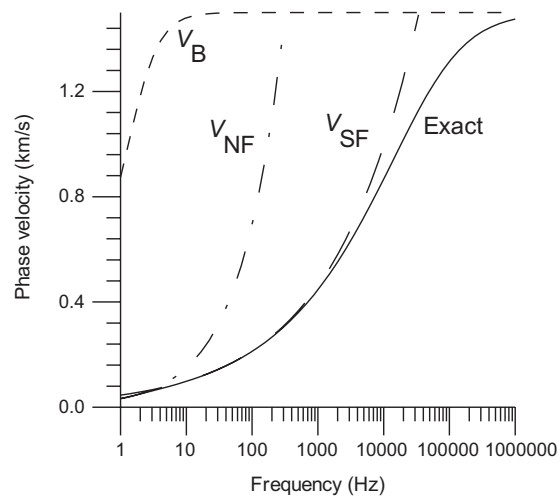

Figure 5. Real part of phase velocity of fluid wave in a 10^{-3} m thick fracture as a function of frequency for water (fluid viscosity is 1 cP). The curves marked as on Figure 1. Stoneley wave regime approximates the exact solution at seismic frequencies.

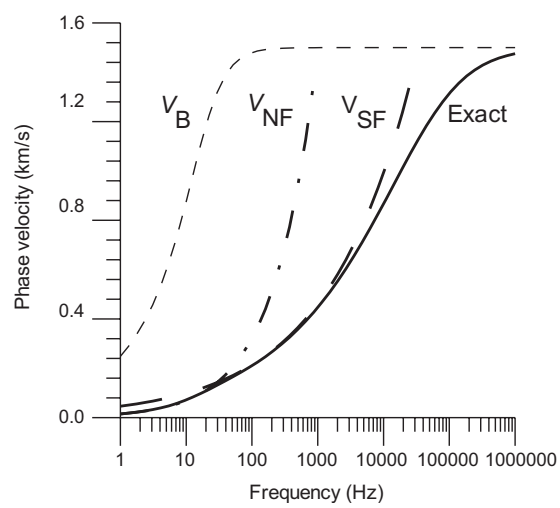

Figure 6. Real part of phase velocity of fluid wave in a 10^{-3} m thick fracture as a function of frequency for the oil (fluid viscosity is 10 cP). The curves marked as on Figure 1. Stoneley wave regime approximates the exact solution at seismic frequencies.

Velocity v_f is directly related to propagation wave number k_z through the expression $v_f = \frac{\omega}{k_z}$, parameters α_{Pj}, α_{Sj} are defined through the formula

$$\alpha_{pj} = \sqrt{k_{pj}^2 - k_z^2}, \quad \alpha_{sj} = \sqrt{k_{sj}^2 - k_z^2}, \quad j = 1,2, \quad (41)$$

and the functions ξ_1, χ_1, ξ_2, and χ_2 have the expressions

$$\xi_1 = \frac{J_1(\alpha_{p1}R)}{J_0(\alpha_{p1}R)}, \quad \chi_1 = \frac{J_1(\alpha_{s1}R)}{J_0(\alpha_{s1}R)}, \quad \xi_2 = \frac{H_1^{(2)}(\alpha_{p2}R)}{H_0^{(2)}(\alpha_{p2}R)}, \quad (42)$$

$$\chi_2 = \frac{H_1^{(2)}(\alpha_{s2}R)}{H_0^{(2)}(\alpha_{s2}R)},$$

where $J_k(Z)$ is a Bessel function and $H_k^{(2)}(Z)$ is a Hankel function of the second kind.

For $|Z| \ll 1$, the asymptotic expressions

$$\frac{J_1(Z)}{J_0(Z)} \approx \frac{Z}{2}\left(1 + \frac{Z^2}{8}\right), \quad \frac{H_1^{(2)}(Z)}{H_0^{(2)}(Z)} \approx -\frac{1}{Z\ln(Z/2)} \quad (43)$$

can be used.

Assuming low enough frequency, when

$$|\alpha_{p1}R| \ll 1, \quad |\alpha_{p2}R| \ll 1, \quad |\alpha_{s2}R| \ll 1, \quad (44)$$

and the asymptotic expressions 43 can be applied to equation 40. This reduces equation 40 to

$$\alpha_{s1}\left[k_z^2\left(\mu_2\frac{2\chi_1}{\alpha_{s1}R} - \mu_2\left(1 + \frac{\alpha_{p1}^2R^2}{8}\right) - \mu_1\right) + k_{p1}^2\left(\lambda_1 + \mu_1 + \mu_2\left(1 + \frac{\alpha_{p1}^2R^2}{8}\right)\right)\right] = 0. \quad (45)$$

Note that according to equation 42, the ratio $\frac{2\chi_1}{\alpha_{s1}R}$ from equation 45 has a limit equal to one if the argument of χ_1 goes to zero, meaning that the pipe radius is much smaller than the wavelength of the shear wave in the fluid.

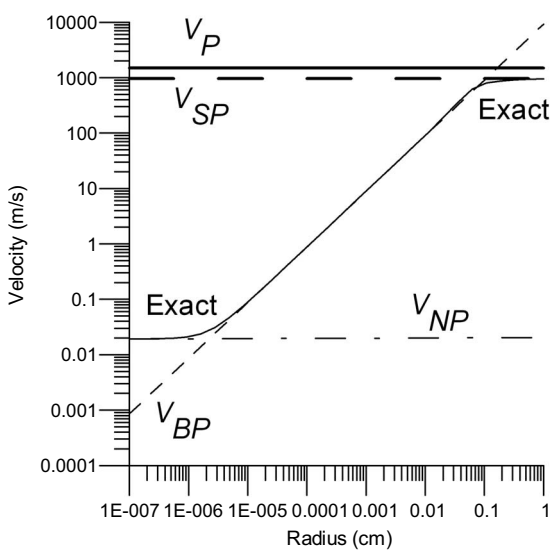

Figure 7. Real part of phase velocity of fluid waves in a pipe filled with oil (fluid viscosity is 10 cP) as a function of pipe radius. Frequency is 20 Hz. Shown are the exact solution (thin solid line) obtained from equation 40, V_{BP} (short dashed line) obtained from equation 52, V_{SP} (long dashed line) obtained from equation 48, V_P (thick solid line, equation 4), and V_{NP} (dashed-dotted line, equation 55).

Factor α_{s1} gives equation 45 an immediate solution for a shear wave in a viscous fluid (equation 5) that is the same as in the fracture case.

At higher frequencies, when

$$|\alpha_{s1}R| \gg 1, \quad (46)$$

and the argument for χ_1 is large (and $\chi_1 \approx i$), the expression within the square brackets of 45 gives

$$\frac{k_z^2}{\sqrt{k_{s1}^2 - k_z^2}} = i\frac{R}{2\eta}[k_{p1}^2(\lambda_1 + \mu_1 + \mu_2) - k_z^2(\mu_1 + \mu_2)], \quad (47)$$

which can be put in the form of a cubic polynomial with respect to k_z^2 and solved explicitly using Cardano formulas. For a small viscosity η, the expression in square brackets must approach zero, and we obtain

$$v_f = V_{SP} \equiv V_P\sqrt{\frac{\mu_1 + \mu_2}{\lambda_1 + \mu_1 + \mu_2}}, \quad (48)$$

which for zero viscosity gives

$$v_f = V_P\sqrt{\frac{\mu_2}{\lambda_1 + \mu_2}}, \quad (49)$$

which is the velocity of the Stoneley (tube) wave (White, 1965), propagating along a well filled with fluid.

When $|\alpha_{s1}R| \ll 1$, then approximation 43 can be used for χ_1 and leads to the following quadratic equation with respect to k_z^2:

$$k_z^2 = \frac{8k_{p1}^2(\lambda_1 + \mu_1 + \mu_2)}{R^2\mu_2(k_{s1}^2 - 2k_{p1}^2) - \mu_1}. \quad (50)$$

Introducing a dimensionless real parameter

$$p = \frac{R^2\mu_2\rho_f}{8\eta^2}, \quad (51)$$

that determines the main component in the denominator of equation 50, we find that when $p \gg 1$, then the module of the square of the coefficient for k_z^2 is much larger than the module of the last term. Thus, for $p \gg 1$, from equation 50, we obtain

$$v_f = V_{BP} \equiv V_P\sqrt{\frac{\mu_2}{\lambda_1 + \mu_2}}\sqrt{\frac{-i\omega\kappa_c\rho_f}{\eta}}, \quad (52)$$

where $\kappa_c = \frac{R^2}{8}$ is pipe permeability. This wave has a velocity close to that of the slow fluid wave (Appendix B) for a cylinder with the "Stoneley" correction factor $\sqrt{\frac{\mu_2}{\lambda_1 + \mu_2}}$. If the rigidity of the fluid goes to zero, then v_f (equation 52) approaches the solution from Appendix B), and

$$v_f = V_P\sqrt{\frac{-i\omega\kappa_c\rho_f}{\eta}}. \quad (53)$$

When

$$\sqrt{\frac{\omega\kappa_c\rho_f}{\eta}} > 1, \quad (54)$$

the fluid wave velocity becomes nondispersive and propagates as a tube wave described by equation 49.

When $p \ll 1$ (small pipe radius), then from equation 50 we have

$$v_f = V_{NP} \equiv V_P\sqrt{\frac{-i\omega\eta}{\lambda_1 - i\omega\eta + \mu_2}}. \quad (55)$$

Regimes V_{SP}, V_{BP}, and V_{NP} for the pipe relate, respectively, to the regimes V_{SF}, V_{BF}, and V_{NF} derived for a fracture earlier in this paper. The presence of character P in the subscript indicates the regime for a pipe model.

NUMERICAL RESULTS FOR A PIPE

The main idea behind the numerical study of wave propagation in a pipe is the same as that for a fracture, which is to evaluate the validity of derived asymptotics for realistic rock parameters. The exact solution was obtained by the direct root search of equation 40, which, as in the case of fractures, revealed the existence of two roots. One of the roots corresponds to the velocity of shear waves in the fluid; the other root represents the symmetric fluid wave, which propagates in different regimes, depending on the parameter values. For all data presented here $c_P = 1500$ m/s, $V_{P2} = 1800$ m/s, $V_{S2} = 800$ m/s, $\rho_2 = 2.7$ g/cm^3, and fluid viscosity $\eta = \varsigma = 10$ cP (oil). Figure 7 shows the phase velocities for a pipe as a function of the pipe radius R for 20 Hz frequency. Also shown are V_{P1}, V_{SP}, V_{BP}, and V_{NP}. Figure 8 shows phase velocities as a function of frequency for a pipe with 10^{-4} m radius, while Figure 9 presents computations for a thinner pipe with 10^{-8} m radius.

DISCUSSION

Theoretical and numerical results presented in this study reveal several similarities in wave propagation between a fracture and a pipe. The fluid symmetrical wave is always present in the solution, and it can propagate in different regimes. The first regime, described by V_{SF} (equation 25 for a fracture) and V_{SP} (equation 48 for a pipe), can be called a Stoneley regime. Ferrazzini and Aki (1987) found that their solution (which has V_{S0} from equation 18, as a low-frequency asymptote) approaches to propagation of Stoneley waves for a solid-fluid plane interface as the fracture thickness grows. At the same time, the Stoneley (tube) wave character of the solution V_{SP} is a well-recognized fact (White, 1965). Velocities of these waves directly depend on fluid viscosity, frequency, and the shear modulus of the walls; consequently, wall elasticity is an important parameter here.

The second regime is represented by V_{BF} (equation 30 for a fracture) and V_{BP} (equation 53 for a pipe) and can be called a Biot regime. The relationship of solutions representing both the Biot propagation regime and the Biot slow wave in poroelastic theory follows from the similarity in asymptotic expressions for these waves at low frequencies as well as from assumptions used for deriving dynamic poroelastic equations. When modeling an interaction force between fluid and elastic components at pore scale, Biot (1956b) first considers the oscillatory flow of fluid between two rigid parallel walls, which is the same problem for the low-frequency solution considered in Korneev (2008), using a somewhat different technique. In the next section of the same paper, Biot solves the analogous problem for a cylindrical tube (see Appendix B). Then, Biot calculates a friction force acting between fluid and elastic skeleton using "the assumption that the variation of friction with frequency follows the same laws as found in the foregoing for the tube of uniform cross section" (Biot, 1956b, p. 182). At low frequencies, the solutions for the Biot's second slow wave in a poroelastic material (equation C-1), and Biot regimes for the fracture (equation 30) and a pipe (equation 53) have the same dependence on frequency, permeability, fluid density, and fluid viscosity, in the form

$$V_f = V\sqrt{\frac{-i\omega\kappa\rho_f}{\eta}} \tag{56}$$

where V is some velocity, which is independent of any parameters under the radical, κ is permeability of the porous media, $\kappa = \frac{h^2}{12}$ for a fracture, and $\kappa = \frac{R^2}{8}$ for a pipe.

The third regime described by V_{NF} (equation 27 for a fracture) and V_{NP} (equation 54 for a pipe) occurs at very small scales, when channel width is much smaller than the skin depth, and can be called a *narrow channel* regime. These waves propagate by squeezing in fluid through the narrow channels of fractures and pipes when the wavelength of the shear wave in the fluid is larger than the channel width. In this regime, the waves also quickly dissipate. This is generally a rather slow wave, but it can be faster than the other fluid wave (e.g., the shear fluid wave), depending on the parameters (see Figure 9).

A Stoneley wave propagation regime is very different for the considered geometries. In a pipe with a large radius (or in absence of viscosity) at low frequencies, the Stoneley wave has virtually no dispersion propagating as a tube wave. By contrast, in a fracture, the Stoneley guided wave has a strong dispersion. In a pipe, the Stoneley wave regime converts to a Biot-wave regime quite rapidly, as soon as the condition

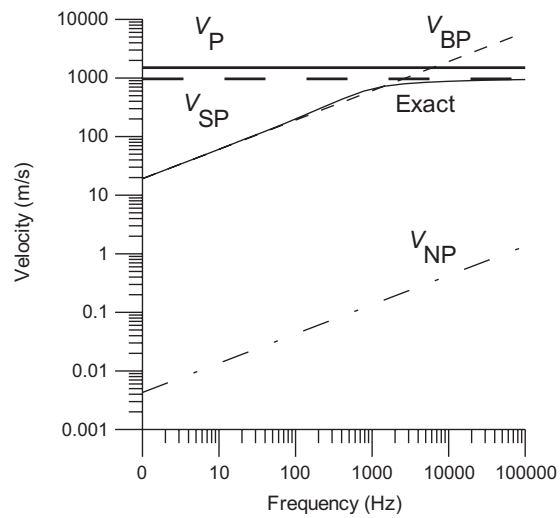

Figure 8. Real part of phase velocity of fluid waves in a pipe filled with oil (fluid viscosity is 10 cP) as a function of frequency. Pipe radius is 10^{-4} m. The curves marked as on Figure 7.

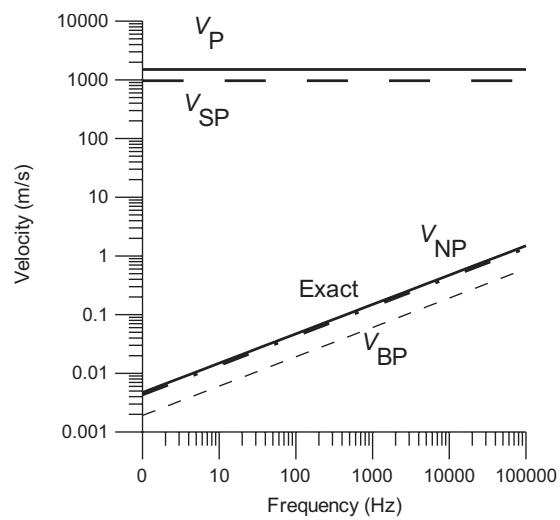

Figure 9. Real part of phase velocity of fluid waves in a pipe filled with oil (fluid viscosity is 10 cP) as a function of frequency. Pipe radius is 10^{-8} m. The curves marked as on Figure 7.

$$\sqrt{\frac{\omega\kappa_c\rho_f}{\eta}} > 1 \tag{57}$$

is valid. In a fracture, the Biot wave regime can be achieved for the high-contrast cases only when the fluid is in a gaseous state. A quite common derivation of the Biot regime occurs when the rigidity of the walls is placed at infinity (e.g., Chang et al., 1988). Such an assumption is hard to justify from the physical point of view. Indeed, common densities and shear-wave velocities for known rock differ in density and sound wave velocity in water by a factor of 2–3, which is far from the high-contrast assumption between the channel walls and the fluid. Such a contrast can be achieved by applying the theory to a gas only, but this restriction is too severe for poromechanical applications.

Although having some aforementioned similarity, the narrow channel regimes described by equations 27 and 54 differ in their dependence on fluid viscosity. In a fracture, this regime starts relatively quickly as the fracture thickness decreases, while for realistic parameters in pipes, it takes place surprisingly at a nano-scale level (the pipe radius is 10^{-8} m for the example on Figure 9) at seismic frequencies. For liquids, wall rigidity is always a factor affecting wave propagation.

The considered problems have just one fluid-channeling element, taken as infinitely spreading in one or two directions. Real rock contains a wide variety of pores and fractures that can intersect and are distributed in sizes and shapes that provide conditions for different fluid wave regimes. The fractal character of fracture and pore distribution in rock suggests a rapid increase in their numbers for decreasing length scales. Diffusion waves are slow and propagate short distances, but the abundance of both small-scale channels and reflection-refraction on rock heterogeneities, where diffusion waves can directly impact boundary conditions, can possibly make significant contributions to overall wave propagation. (Accurate consideration of all wave propagation effects in such media is a very complex problem, one that is beyond the scope of this study.)

The hydrogeology results provide strong evidence that fractures play a key role in rock permeability. Permeability was measured for a wide range of scales in a number of comprehensive studies for a variety of geologic environments. Typically, five-orders-of-scale increase corresponds to 5–7 orders of permeability increase, suggesting the dominant role of fractures in fluid flow at field scales.

CONCLUSIONS

Analytical solutions have been obtained for the phase velocities of fluid waves within both an infinite fracture and a pipe filled with a viscous fluid at low frequencies. Two fluid waves can coexist in such objects: a diffusive wave propagating with shear-wave velocity in the fluid and a general fluid wave that can propagate in different regimes, depending on object parameters. These include Biot, Stoneley, and "narrow channel" wave regimes. Computations for realistic rock parameters suggest that for pipes, the most common regime is the Biot slow wave; for fractures, it is the Stoneley (guided) wave. Stoneley guided waves have a strong energy-trapping ability; including these effects into poroelastic theories needs to be considered.

ACKNOWLEDGMENTS

This work was supported by the U. S. Department of Energy under Contract No. DE-AC02-05CH11231. Andrey Bakulin, Dmitry Silin, Gennady Goloshubin, German Maximov, and an anonymous reviewer have made many helpful comments.

APPENDIX A

CYLINDRICAL VECTOR SYSTEM

The cylindrical vector system used in this paper was introduced by Korneev and Johnson (1993). Use of those vectors makes expressions for the Lamé equation especially simple since they thoroughly imply a special symmetry of the problem. They allow formulation of wave propagation problems in displacements, avoiding the potentials.

The cylindrical vector system has the form

$$\mathbf{Y}_m^0 = Y_m\mathbf{e}_3, \quad \mathbf{Y}_m^+ = \frac{1}{2}(Y_m\mathbf{e}_1 - iY_m\mathbf{e}_2), \tag{A-1}$$

$$\mathbf{Y}_m^- = \frac{1}{2}(Y_m\mathbf{e}_1 + iY_m\mathbf{e}_2),$$

where

$$Y_m \equiv Y_m(\varphi,z) \equiv \exp i(m\varphi - h_z z), \quad m = 0,1,2,\ldots, \tag{A-2}$$

and h_z is the projection of the wavenumber onto the OZ-axis, $i = \sqrt{-1}$. Vectors $\mathbf{e}_1,\mathbf{e}_2,\mathbf{e}_3$ are the natural unit vectors of the cylindrical coordinate system (r,φ,z).

The cylindrical vectors of the system in A-1 are orthonormal at any point on a cylindrical surface. In the space of vector functions $\vec{f}(\varphi), 0 \le \varphi \le 2\pi$ defined on a circle $r = const.$, $z = const.$ the vectors A-1 satisfy the following orthogonality relations

$$\int_0^{2\pi} (\mathbf{Y}_m^\nu \cdot \bar{\mathbf{Y}}_{m_1}^{\nu_1}) d\varphi = \delta_{mm_1}\delta_{\nu\nu_1}, \quad \nu = 0,+,- \tag{A-3}$$

where δ_{kl} is equal to 1, when lower indexes are the same, and equal zero otherwise.

The system A-1 is complete in the sense of convergence in the mean for a Fourier series expansion. This means that any vector function

$$\vec{u} \equiv \vec{u}(r,\varphi,z) = \vec{U}(r,\varphi)\exp(-ih_z z) \tag{A-4}$$

can be represented in the form

$$\vec{u}(r,\varphi,z) = \sum_\nu \sum_{m=0}^{\infty} f_m^\nu(r)\mathbf{Y}_m^\nu(\varphi,z). \tag{A-5}$$

The Lamé equation for a homogenous elastic medium is

$$(\lambda+\mu)\nabla\nabla\cdot\vec{u} - \mu\nabla\times\nabla\times\vec{u} + \rho\omega^2\vec{u} = 0 \tag{A-6}$$

where the dependence of the displacement field $\vec{u}$ on time t is given by $\exp(i\omega t)$, where ω is the angular frequency. The parameters λ and μ from A-6 are the Lamé constants, and ρ is the density. Substitution

of the form A-5 into equation A-6 and use of the orthogonality property A-3 yields the differential Bessel equations for radial functions $f_m^\nu \equiv f_m^\nu(r)$:

$$f_{mq}^0 = d_{mq}^0 Z_m(\alpha_q r), \quad f_{mq}^+ = d_{mq}^+ Z_{m+1}(\alpha_q r), \tag{A-7}$$

$$f_{mq}^- = d_{mq}^- Z_{m-1}(\alpha_q r), \quad q = p,s,$$

where $Z_k(x)$ are the cylindrical Bessel functions of order k, and d_{mq}^ν are the arbitrary constants. The parameter α_q from equation A-7 has two forms:

$$\alpha_p = \sqrt{k_p^2 - h_z^2}, \quad \alpha_s = \sqrt{k_s^2 - h_z^2}, \tag{A-8}$$

where $k_p = \omega/\mathrm{v_p}$, $k_s = \omega/\mathrm{v_s}$

$$\mathrm{v_p} = \sqrt{(\lambda + 2\mu)/\rho}, \quad \text{and } \mathrm{v_s} = \sqrt{\mu/\rho} \tag{A-9}$$

are the propagation velocities of compressional ($\vec{u}_p$) and shear ($\vec{u}_s$) field components.

The simplicity of equation A-7 illustrates the main advantage of employing the cylindrical vectors of the form A-1. In other systems, the expressions for radial functions contain combinations of Bessel functions and their derivatives.

Introduction of functions

$$\psi_{mp} = Y_m(\varphi,z)Z_m(\alpha_p r) \quad \text{and } \psi_{ms} = Y_m(\varphi,z)Z_m(\alpha_s r) \tag{A-10}$$

allows representation of the field $\vec{u}$ from equation A-7 in the form

$$\vec{u}(\rho,\varphi,z) = \sum_{m=0}^{\infty} (a_m \mathbf{P}^{(m)} + b_m \mathbf{S}_\mathrm{V}^{(m)} + c_m \mathbf{S}_\mathrm{H}^{(m)}) \tag{A-11}$$

containing the canonical compressional p- waves

$$\begin{aligned}\mathbf{P}^{(m)} &= -\nabla\psi_{mp} = ih_z Z_m \mathbf{Y}_m^0 + \alpha_p Z_{m+1}\mathbf{Y}_m^+ - \alpha_p Z_{m-1}\mathbf{Y}_m^- \\ &= \left(-\alpha_p Z_m' \mathbf{e}_1 - \frac{im}{r} Z_m \mathbf{e}_2 + ih_z Z_m \mathbf{e}_3\right) Y_m\end{aligned} \tag{A-12}$$

and two sets of shear s- waves

$$\begin{aligned}\mathbf{S}_\mathrm{V}^{(m)} &= \nabla\times\psi_{ms}\mathbf{e}_3 = i\alpha_s(Z_{m+1}\mathbf{Y}_m^+ + Z_{m-1}\mathbf{Y}_m^-) \\ &= \left(\frac{im}{r} Z_m \mathbf{e}_1 - \alpha_s Z_m' \mathbf{e}_2\right) Y_m,\end{aligned} \tag{A-13}$$

$$\begin{aligned}\mathbf{S}_\mathrm{H}^{(m)} &= \frac{1}{\alpha_s}\nabla\times\nabla\times\psi_{ms}\mathbf{e}_3 \\ &= \alpha_s Z_m \mathbf{Y}_m^0 + ih_z Z_{m+1}\mathbf{Y}_m^+ - ih_z Z_{m-1}\mathbf{Y}_m^- \\ &= \left(-ih_z Z_m' \mathbf{e}_1 + \frac{mh_z}{\alpha_s r} Z_m \mathbf{e}_2 + \alpha_s Z_m \mathbf{e}_3\right) Y_m.\end{aligned} \tag{A-14}$$

In expressions, the Bessel functions and their derivatives have arguments $\alpha_p r$ and $\alpha_s r$ correspondently for compressional $\mathbf{P}^{(m)}$ and shear $\mathbf{S}_\mathrm{V}^{(m)}$,$\mathbf{S}_\mathrm{H}^{(m)}$ fields, which satisfy the equations

$$\nabla\times\mathbf{P}^{(m)} = 0, \quad \nabla\cdot\mathbf{S}_\mathrm{V}^{(m)} = \nabla\cdot\mathbf{S}_\mathrm{H}^{(m)} = 0, \quad (\mathbf{S}_\mathrm{V}^{(m)}\cdot\mathbf{S}_\mathrm{H}^{(m)}) = 0. \tag{A-15}$$

When $h = 0$, the field $\mathbf{S}_\mathrm{H}^{(m)}$ is polarized along OZ axis, while polarization of $\mathbf{S}_\mathrm{V}^{(m)}$ is always orthogonal to this axis.

For any integer index $m = 0, \pm 1, \pm 2, \ldots$ the fields $\mathbf{P}^{(m)}$, $\mathbf{S}_\mathrm{V}^{(m)}$, and $\mathbf{S}_\mathrm{H}^{(m)}$ satisfy equation of motion A-6, and represent an independently propagating harmonic of this index.

The expressions for the traction field on a surface $r = const.$

$$\mathbf{t}_r(\vec{u}) = \lambda\nabla\cdot\vec{u}\mathbf{e}_1 + \mu\left(2\frac{\partial\vec{u}}{\partial r} + \mathbf{e}_1\times\nabla\times\vec{u}\right) \tag{A-16}$$

have forms:

$$\begin{aligned}\mathbf{t}_r(\mathbf{P}^{(m)}) &= 2i\mu\alpha_p h_z Z_m' \mathbf{Y}_m^0 + \left(\frac{\lambda}{2}k_p^2 Z_m + \mu\alpha_p{}^2 Z_{m+1}'\right)\mathbf{Y}_m^+ \\ &\quad + \left(\frac{\lambda}{2}k_p^2 Z_m - \mu\alpha_p{}^2 Z_{m-1}'\right)\mathbf{Y}_m^- \\ &= [(\lambda k_p^2 Z_m + \mu\alpha_p{}^2(Z_{m+1}' - Z_{m-1}'))\mathbf{e}_1 \\ &\quad - i\mu\alpha_p{}^2(Z_{m+1}' + Z_{m-1}')\mathbf{e}_2 + 2i\mu\alpha_p h_z Z_m' \mathbf{e}_3]Y_m\end{aligned} \tag{A-17}$$

$$\begin{aligned}\mathbf{t}_r(\mathbf{S}_\mathrm{V}^{(m)}) &= \mu\left(\frac{mh_z}{r} Z_m \mathbf{Y}_m^0 + i\alpha_s{}^2\left(Z_{m+1}' - \frac{Z_m}{2}\right)\mathbf{Y}_m^+\right. \\ &\quad \left. + i\alpha_s{}^2\left(Z_{m-1}' - \frac{Z_m}{2}\right)\mathbf{Y}_m^-\right) \\ &= \mu\left[i\alpha_s^2(Z_{m+1}' + Z_{m-1}')\mathbf{e}_1 + \alpha_s\left(\alpha_s Z_{m+1}'\right.\right. \\ &\quad \left.\left. - \frac{m-1}{r} Z_{m-1}\right)\mathbf{e}_2 + \frac{mh_z}{r} Z_m \mathbf{e}_3\right] Y_m\end{aligned} \tag{A-18}$$

$$\begin{aligned}\mathbf{t}_r(\mathbf{S}_\mathrm{H}^{(m)}) &= \mu((2\alpha_s{}^2 - k_s^2)Z_m' \mathbf{Y}_m^0 + ih_z\alpha_s Z_{m+1}' \mathbf{Y}_m^+ \\ &\quad - ih_z\alpha_s Z_{m-1}' \mathbf{Y}_m^-) \\ &= \mu[ih_z\alpha_s(Z_{m+1}' - Z_{m-1}')\mathbf{e}_1 + h_z\alpha_s(Z_{m+1}' \\ &\quad + Z_{m-1}')\mathbf{e}_2 + (2\alpha_s{}^2 - k_s^2)Z_m' \mathbf{e}_3]Y_m\end{aligned} \tag{A-19}$$

APPENDIX B

SLOW FLUID WAVE FOR A PIPE

Consider equation 3 in a cylindrical coordinate system and use the rigid wall assumption. In such a model, the interaction between walls and the fluid occurs through viscous friction forces. At low frequencies, the fluid motion is mostly directed along the central axis with a parabolic distribution across the fracture, which reaches the maximum at the center line z = 0 and zero at the walls, so

$$\mathbf{u} \approx u_z \mathbf{z}_1 = u_0(R^2 - r^2)\mathbf{z}_1, \quad u_0 = \text{const.} \tag{B-1}$$

Introducing the total flow

$$F = 2\pi \int_0^R u_z r dr \tag{B-2}$$

across any $z = \text{const}$, reduces equation 3 to

$$\frac{\partial^2 F}{\partial t^2} + \frac{8\eta}{R^2 \rho_f}\frac{\partial F}{\partial t} - \frac{1}{\rho_f}\left(\zeta + \frac{4\eta}{3}\right)\frac{\partial^2}{\partial z^2}\frac{\partial F}{\partial t} - c_P^2 \frac{\partial^2 F}{\partial z^2} = 0. \tag{B-3}$$

Note that pipe permeability is $\kappa_c = R^2/8$; therefore, it is embedded in the denominator of the second term of equation B-2. (Compare to a fracture permeabilty $\kappa_{fr} = h^2/12$). In the frequency domain, equation B-3 has the solution (Korneev et al., 2004)

$$u = \exp i(kx - \omega t), \tag{B-4}$$

with the complex wavenumber k, and the angular frequency ω. The wavenumber has the form

$$k = \frac{\omega}{c_P}\sqrt{\frac{1 + id}{1 - ig}}, \tag{B-5}$$

where

$$d = \frac{\eta}{\omega \kappa_c \rho_f}, \quad g = \frac{\omega\left(\zeta + \frac{4\eta}{3}\right)}{\rho_f c_P^2}. \tag{B-6}$$

At low frequency, the phase velocity V_{f} of the wave described by equation B-4 has the asymptotic form

$$V_{\mathrm{f}} = c_P \sqrt{\frac{-i\omega\kappa_c\rho_f}{\eta}} \tag{B-7}$$

APPENDIX C

BIOT SLOW WAVE AT LOW FREQUENCY

Low-frequency asymptotic for the Biot slow wave can be found in the original papers (Biot, 1956a, b). Since then, numerous papers dealing with Biot's poroelastic equations were published. For example, in more contemporary notations, this equation can be found in Dutta and Ode (1979). Slightly changing their notations (in order to avoid interference with those used in the main text), one can obtain a low-frequency asymptotic for Biot's slow wave in the form

$$V_f = \sqrt{\frac{2D(2DG^2 - H)}{H}}\sqrt{\frac{-i\omega\kappa\rho_f}{\eta}}, \tag{C-1}$$

where η is a fluid shear viscosity, ω is an angular frequency, ρ_f is fluid density and κ is a permeability of the rock. Parameters

$$D = \frac{K_s}{2}\left[G + \frac{\phi}{K_f}(K_s - K_f)\right]^{-1}, \tag{C-2}$$

$$H = \lambda + 2\mu, \tag{C-3}$$

$$G = 1 - \frac{K_m}{K_s}. \tag{C-4}$$

from equation C-1 depend on the bulk moduli K_s, K_f, and K_m of the discrete solid grains; the fluid, and the matrix, respectively; Lame constants of the fluid-filled matrix λ and μ; and porosity ϕ.

REFERENCES

Abramowitz, M., and I. A. Stegun, 1972, Handbook of mathematical functions with formulas, graphs, and mathematical tables: Dover.

Biot, M. A., 1956a, Theory of propagation of elastic waves in a fluid-saturated porous solid. I. Low-frequency range: The Journal of the Acoustical Society of America, **28**, no. 2, 168–178.

Biot, M. A., 1956b, Theory of propagation of elastic waves in a fluid-saturated porous solid. II. Higher frequency range: The Journal of the Acoustical Society of America, **28**, no. 2, 179–191.

Burridge, R., S. Kostek, and A. L. Kurkjian, 1993, Tube waves, seismic waves, and effective sources: The Journal of the Acoustical Society of America, **93**, no. 4, 2396–2396.

Chang, S. K., H. L. Liu, and D. L. Johnson, 1988, Low-frequency tube waves in permeable rocks: Geophysics, **53**, 519–527.

Cheng, C. H., and M. N. Toksoz, 1981, Elastic wave propagation in a fluid-filled borehole and synthetic acoustic logs: Geophysics, **46**, 1042–1053.

Chouet, B., 1988, Resonance of a fluid-driven crack: Radiation properties and implication for the source of long-period events and harmonic: Journal of Geophysical Research, **93**, B5, 4375–4400.

Chouet, B., 1986, Dynamics of a fluid-driven crack in three dimensions by the finite-difference method: Journal of Geophysical Research, **91**, B14, 13967–13992.

Derov, A., G. Maximov, M. Lazarkov, B. Kashtan, and A. Bakulin, 2009, Characterizing hydraulic fractures using slow waves in the fracture and tube waves in the borehole, 79th Annual International Meeting, SEG, Expanded Abstracts, 4115–4119.

Dutta, N. C., and H. Ode, 1979, Attenuation and dispersion of compressional waves in fluid-filled porous rocks with partial gas saturation (White model) — Part I: Biot theory: Geophysics, **44**, 1777–1788.

Ferrazzini, V., B. Chouet, M. Fehler, and K. Aki, 1990, Quantitative analysis of long-period events recorded during hydrofracture experiments at Fenton Hill, New Mexico: Implications for volcanic tremor: Journal of Geophysical Research, **95**, B13, 21871–21884.

Ferrazzini, V., and K. Aki, 1987, Slow waves trapped in a fluid-filled infinite crack: Implications for volcanic tremor: Journal of Geophysical Research, **92**, B9, 9215–9223.

Frehner, M., and S. Schmalholz, 2010, Finite-element simulations of Stoneley guided wave reflection and scattering at the tips of fluid-filled fractures: Geophysics, **75**, no. 2, T23–T36.

Goloshubin, G. M., P. V. Krauklis, L. A. Molotkov, and H. B. Helle, 1994, Slow wave phenomenon at seismic frequencies: 64th Annual International Meeting, SEG, Expanded Abstracts, 809–811.

Groenenboom, J., and J. Falk, 2000, Scattering by hydraulic fractures: Finite-difference modeling and laboratory data: Geophysics, **65**, 612–622.

Groenenboom, J., and D. B. van Dam, 2000, Monitoring hydraulic fracture growth: Laboratory experiments: Geophysics, **65**, 603–611.

Groenenboom, J., and J. T. Fokkema, 1998, Guided waves along hydraulic fractures: 68th Annual SEG Meeting, Expanded Abstracts.

Haddon, R. A. W., 1989, Exact Green's functions using leaking modes for axisymmetric boreholes in solid elastic media: Geophysics, **54**, 609–620.

Hornby, B. E., D. L. Johnson, K. W. Winkler, and R. A. Plumb, 1989, Fracture evaluation using reflected Stoneley-wave arrivals: Geophysics, **54**, 1274–1288.

Korneev, V., A. Ponomarenko, and B. Kashtan, 2009, Stoneley guided waves: What is missing in Biot's theory? Proceedings of the Forth Biot Conference on Poromechanics: DEStech Publication Inc., 706–711.

Korneev, V. A., 2008, Slow waves in fractures filled with viscous fluid: Geophysics, **73**, no. 1, N1–N7.

Korneev, V. A., G. M. Goloshubin, T. V. Daley, and D. B. Silin, 2004, Seismic low-frequency effects in monitoring of fluid-saturated reservoirs: Geophysics, **69**, 522–532.

Kostek, S., D. L. Johnson, and C. J. Randall, 1998a, The interaction of tube waves with borehole fractures. Part I: Numerical models: Geophysics, **63**, 800–808.

Kostek, S., D. Johnson, L. Winkler, and B. E. Hornby, 1998b, The interaction of tube waves with borehole fractures, Part II: Analytical models: Geophysics, **63**, 809–815.

Krauklis, P. V., 1962, About some low frequency oscillations of a liquid layer in elastic medium: Prikladnaya Matematika i Mekhanika, **26**, 1111–1115 (in Russian).

Norris, A., 1989, Stoneley wave attenuation and dispersion in permeable formations: Geophysics, **54**, 330–341.
Norris, A., 1987, The tube wave as a Biot slow wave: Geophysics, **52**, 694–696.
Paillet, F. L., and J. E. White, 1982, Acoustic models of propagation in the borehole and their relationship to rock properties: Geophysics, **47**, 1215–1228.
Schoenberg, M., T. Marzetta, J. Aron, and R. P. Porter, 1981, Space-time dependence of acoustic waves in a borehole: The Journal of the Acoustical Society of America, **70**, no. 5, 1496–1507.
Tang, X. M., and C. H. Cheng, 1988, Wave propagation in a fluid-filled fracture — an experimental study: Geophysical Research Letters, **15**, no. 13, 1463–1466.
White, J. E., 1965, Seismic waves: Radiation, transmission, and attenuation: McGraw-Hill Book Co.
Yamamoto, M., and H. Kawakatsu, 2008, An efficient method to compute the dynamic response of a fluid-filled crack: Geophysical Journal International, **174**, no. 3, 1174–1186.
Ziatdinov, S., A. Bakulin, and B. Kashtan, 2006, Tube waves from a horizontal fluid-filled fracture of a finite radius: 76th Annual International Meeting, SEG, Expanded Abstracts, 369–372.